Active and passive protection of AA2024-T3 by a hybrid inhibitor doped mesoporous sol-gel and top coating system

Recloux, I; Gonzalez Garcia, Y; Druart, ME; Khelifa, F; Dubois, P; Mol, JMC; Olivier, MG

DOI
10.1016/j.surfcoat.2015.11.002

Publication date
2016

Document Version
Final published version

Published in
Surface and Coatings Technology

Surface & Coatings Technology 303 (2016) 352–361

Contents lists available at ScienceDirect

Surface & Coatings Technology

journal homepage: www.elsevier.com/locate/surfcoat

Active and passive protection of AA2024-T3 by a hybrid inhibitor doped mesoporous sol–gel and top coating system

I. Recloux [a,*], Y. Gonzalez-Garcia [b], M.-E. Druart [a], F. Khelifa [c], Ph. Dubois [c], J.M.C. Mol [b], M.-G. Olivier [a]

[a] Materials Science Department, Research Institute for Materials Science and Engineering, University of Mons, Place du Parc 20, 7000 Mons, Belgium
[b] Department of Materials Science and Engineering, Delft University of Technology, Mekelweg 2, 2628CD Delft, The Netherlands
[c] Laboratory of Polymeric and Composite Materials, Research Institute for Materials Science and Engineering, University of Mons, Place du Parc 20, 7000 Mons, Belgium

ARTICLE INFO

Article history:
Received 15 July 2015
Revised 30 October 2015
Accepted in revised form 1 November 2015
Available online 10 November 2015

Keywords:
Self-healing
Mesoporous film
Inhibitor
Corrosion protection
Scanning electrochemical microscopy
Electrochemical micro-cell

ABSTRACT

In the present investigation, a two-layer coating system was developed in order to protect 2024 aluminium alloy against corrosion. At the metal interface, a silica mesoporous thin film was used to offer storage and release functionalities for benzotriazole inhibitive molecules (active protection). An acrylic top coat was then applied as a barrier layer against corrosive species (passive protection). Various electrochemical techniques were employed to evaluate the anticorrosion performance of the coating system. Amongst them, the scanning vibrating electrode technique (SVET) and the scanning electrochemical microscopy (SECM) showed a slowdown of corrosion processes occurring within the damaged coating area. The acquisition of anodic polarization curves inside the scratch through the use of an electrochemical micro-cell allowed to correlate this enhancement in the corrosion protection with the formation of an inhibitive film. Upon a through-coating damage, the mesoporous reservoir comes into contact with the aggressive electrolyte and benzotriazole molecules are able to be released and to inhibit corrosion of the bare metal exposed in the scratch. The work demonstrates the potential of mesoporous films as reservoir for inhibitive species and its efficiency for controlled release of the inhibitor. Furthermore, the work demonstrates the added value of electrochemical micro-cell measurements to highlight active corrosion protection in coating defects due to inhibitor doped coating systems.

1. Introduction

The development of environmentally friendly protective coating systems for 2024 aluminium alloy (AA2024) is a concern of prime importance for the aerospace industry. Until now, hexavalent chromium based pretreatment and primer coating systems have traditionally been used for the corrosion protection of AA2024 [1]. However, the European regulation REACH (Registration, Evaluation, Authorization and Restriction of Chemicals) has planned the complete prohibition of hexavalent chromium in this industry as from 2017 due to its toxicity for health and environment [2], unless an authorization has been granted to the user or the upstream manufacturer/importer. Authorization applies regardless of the quantity used, and in addition to the REACH registration requirement. Nowadays, it is clear that the introduction of hexavalent chromium free surface protection systems has the highest priority in the aerospace industry. The new generation of coatings has to provide long-term anticorrosion protection to metallic substrates. This performance is related to barrier properties (passive protection) offered by the intact coating system and to its ability to protect the exposed metal surface when defects occur (active protection) [3–5]. One promising method is to use eco-friendly alternative corrosion inhibitors [6–10] in combination with a barrier coating system. Different approaches have already been reported in the literature to introduce inhibitive species in protective coatings including direct addition in the coating formulation [11–17], prior encapsulation in nanocapsules [18–22], halloysites [23–26], ion-exchange nanoclays [3,5,27–30] etc.

A very interesting alternative is the use of a two-layer coating system with each layer playing a unique role in the overall protection scheme: active and passive functionalities. Ferreira et al. [31] reported a two-step pretreatment composed of a rare-earth conversion layer and of a sol–gel film. The first layer was the corrosion inhibitor reservoir while the sol–gel coating provided a barrier against the aggressive solution. Some authors [32] also applied a multi-layered hybrid inorganic–organic sol–gel coating with a structure composed of an intermediate cerium layer deposited between two undoped layers. It was shown that the presence of the intermediate layer enhances the metal protection. More recently, Lamaka et al. developed a new strategy for incorporating corrosion inhibitors [33,34]. They used a layer of TiO_x porous nanoparticles as

* Corresponding author.
E-mail addresses: isaline.recloux@umons.ac.be (I. Recloux), Y.GonzalezGarcia@tudelft.nl (Y. Gonzalez-Garcia), marie-eve.druart@umons.ac.be (M.-E. Druart), farid.khelifa@umons.ac.be (F. Khelifa), philippe.dubois@umons.ac.be (P. Dubois), J.M.C.Mol@tudelft.nl (J.M.C. Mol), marjorie.olivier@umons.ac.be (M.-G. Olivier).

http://dx.doi.org/10.1016/j.surfcoat.2015.11.002
0257-8972/

reservoir for organic corrosion inhibitors and then a classical sol–gel coating as barrier protection. The system was particularly efficient to provide self-healing ability and long-term active protection to 2024 aluminium alloy.

In this work, a mesoporous silica sol–gel thin film doped with benzotriazole was firstly applied by dip coating on AA2024 to offer a reservoir and release functionality for corrosion inhibitors (active protection). Then an acrylic top coat was deposited by spin coating on the top of the doped mesoporous film to confine the corrosion inhibitor inside the mesoporosity and to prevent the diffusion of aggressive species through the coating system (passive or barrier protection) [35]. Benzotriazole was selected for its high inhibitive efficiency on AA2024. The compound forms a film by adsorption on the alloy surface providing anticorrosion properties. Benzotriazole molecules adsorbed on the metal decrease the rate of both anodic and cathodic reactions occurring during the corrosion process [36–38]. A long-term corrosion protection of AA2024 is observed in neutral chloride solutions containing a sufficient amount of benzotriazole [39]. The high solubility in water of the compound as well as the fact that it does not specifically interact with the mesoporous silica framework promote its release in solution once the barrier properties of the top coat are damaged [39].

Using a two-layer coating system allows to avoid the deterioration of barrier properties of the coating system and a deactivation of the corrosion inhibitor observed when the latter is directly added in the coating formulation [13,14,16]. Moreover, the dispersion step required with the use of nanocontainers is by-passed and the quantity of inhibitive species is not conditioned by stability issues but only by the porosity of the pretreatment. Finally, the diffusion of active species in the aggressive solution once the coating system is damaged is easier since inhibitive molecules are not entrapped in closed pores or in a cross-linked structure [39].

In light of these numerous developments of smart coatings, several electrochemical methods for the evaluation of the self-healing ability at the microscopic level have also been developed. Amongst them, the scanning electrochemical microscopy (SECM), a powerful technique to monitor in situ corrosion processes due to its high spatial resolution and electrochemical sensitivity, can be mentioned. This technique has already provided very interesting information in the study and the evaluation of defective coating systems [4,40–45]. In particular, the redox competition mode allows to record the cathodic reaction of the corrosion onset taking place within a scratch. The scanning vibrating electrode technique (SVET) can also be mentioned amongst the techniques widely used to study the efficiency of corrosion inhibitors. This in situ technique monitors the distribution of ionic currents arising from the metal surface and provides the opportunity of locating anodic and cathodic areas related to corrosion processes at micrometric resolution [18,21,33,46–48].

The electrochemical micro-cell technique, initially set-up by Suter and Böhni [49], is useful to characterize the microstructure of metals [50–52]. The behaviour of intermetallic particles in aluminium alloys exposed to a solution containing corrosion inhibitors was also studied in some works through this method [7,53–55].

In the present paper, complementary macro- and micro-electrochemical techniques were used to study the protective properties of the mesoporous film and release efficiency of the inhibitor within the defect. The electrochemical impedance spectroscopy (EIS) was employed to get an average information on the protective properties of the coating at the macro-scale. The active protection provided by the two-layer coating system was evaluated using SECM and SVET measurements. Finally, the electrochemical micro-cell was used as a new alternative technique in the evaluation of the active protection offered by a coating system and in the monitoring of the healing process occurring directly in a damaged coating area. The acquisition of local anodic polarization curves on the bare metal exposed in the scribed coating allowed us to monitor the formation of a passive film within the defect.

2. Material and methods

2.1. Materials and sample preparation

The synthesis of the active mesoporous sol–gel pretreatment doped with benzotriazole molecules and its application on AA2024 have already been reported in detail previously [39,56]. Mesoporous films are synthesized by the evaporation induced self-assembly process (EISA). Benzotriazole is post-incorporated inside mesoporous films by impregnation in a solution containing the inhibitor followed by solvent evaporation. The thickness of the film deposited by dip coating process is about 240 nm and its porous structure was fully characterized in previous papers [39,56]. Films showed an important specific surface area (360 m^2/g) and a high open porosity (around 40 vol.%) with an average pore size of 7 nm. The inhibitor loading content was about 8×10^{-7} mol·cm^{-2} inside the film.

The top coat is based on an acrylic copolymer, namely the poly(2-ethylhexyl acrylate(EHA)-*co*-glycidyl methacrylate(GMA)), with a molar ratio in EHA and GMA of 20:80 [35]. This top layer is deposited by spin-coating on the mesoporous pretreatment with a rotation speed of 3000 rpm to obtain acrylic films with a thickness of 1 μm. Thicknesses were checked using a mechanical profilometer. This process was chosen in order to avoid the leakage of benzotriazole during this step. The drying step is achieved at room temperature during 24 h.

It is worth noting that the acrylic top coat selected for this work cannot compete with more advanced top coat systems. The coating thickness is low and no chemical additive is added in the formulation in order to deliberately limit the barrier protection against aggressive species with time and to focus on the active corrosion protection provided by the underlying loaded mesoporous film.

To highlight the contribution of the corrosion inhibitor to protective properties, two types of samples were prepared and tested:

(1) aluminium alloy coated with the mesoporous pretreatment and then coated with the acrylic top coat (undoped coating system); and
(2) aluminium alloy coated with the mesoporous pretreatment, immersed in benzotriazole solution (20 g/L in ethanol), dried at 50 °C during 2 min and then coated with the acrylic top coat (doped coating system).

2.2. Experimental techniques

EIS measurements were performed on uncoated and coated AA2024 samples using a conventional three-electrode set-up. The working electrode was the sample under investigation. The exposed surface area was defined by the diameter of the Plexiglas cell (7 cm^2) used to contain 20 mL of the testing solution (0.05 M NaCl). The counter electrode was a platinum wire and all potentials were measured with respect to an Ag/AgCl/KCl sat. reference electrode (+197 mV/SHE). Samples were placed in a Faraday cage to avoid electromagnetic interferences during measurements. A 5 mV rms sinusoidal perturbation was applied to the open circuit potential in the 10^{-2}–10^5 Hz frequency range. Measurements were performed using an AMETEK Parstat 2273 computer controlled with Powersuite® software.

SECM measurements were carried out with the Scanning Electrochemical Workstation Model 370 (Princeton Applied Research, AMETEK). A platinum-disc microelectrode of 10 μm diameter, an Ag/AgCl,KCl sat. electrode and a platinum plate were used as the working, the reference and the counter electrodes, respectively. Experiments were performed in 0.01 M NaCl solution containing 5 mM ferrocenemethanol. The ferrocenemethanol was used as electrochemical redox mediator. Cyclic voltammograms were recorded at a scan rate of 0.01 V s^{-1} in the bulk solution at the Pt-microelectrode prior to any measurements and after each

scan. The potential was ranged from 0 V (vs Ag/AgCl, KCl sat.) to 0.5 V (vs Ag/AgCl, KCl sat.) to force oxidation of ferrocenemethanol. This step allowed checking the state, i.e. degradation or contamination, of the tip. The dissolved oxygen was used as mediator to establish the tip-sample distance. Approach curves were measured for a tip potential set at −0.77 V (vs Ag/AgCl, KCl sat.) corresponding to the reduction of dissolved oxygen in the solution and were performed sufficiently far from the defective area of the coating. SECM scan measurements were performed in redox competition mode at an identical tip potential and at a tip-sample distance of 100 μm. This height was chosen in order to minimize a local pH change close to the sample surface due to the reduction reaction of dissolved oxygen occurring at the tip [57]. Scan lines and maps were carried out at scan rates of 50 μm s^{-1} and of 100 μm s^{-1} respectively. All the maps were built as a composition of X displacement lines (from left to right), which were stepwise shifted in the Y direction (top-down).

SVET (Applicable Electronics Inc., USA) analyses were performed in 0.01 M NaCl solution. The micro-electrode (MicroProbes Inc., USA) is electroplated with platinum to get a round-shape tip of 20–30 μm diameter. The probe-sample distance was 100 μm. Each map scan took approximately 12 min. Scans were initiated within 5 min of immersion and collected every 2 h for 24 h. A picture of the sample surface was also taken for each scan by a video camera. Plotting of the results was performed by using QuikGrid. To minimize problems of evaporation of the solution a peristaltic pump supplied with demineralized water was used during all SVET measurements.

For SVET and SECM measurements, three samples were scanned for each condition to evaluate the reproducibility. For each case, representative scans were selected for presentation. Prior to analyses, samples were scratched using a scalpel blade to obtain a defect area with a length of about 2 mm and a width of about 70 μm.

The experimental set-up used for electrochemical micro-cell measurements was according to the configuration reported by Suter and Böhni [49]. The micro-cell was a glass microcapillary filled with electrolyte and embedded in a micro-cell which was mounted on the revolving nosepiece of an optical microscope. A silicone gasket was used to seal the glass microcapillary tip and to avoid any solution leakage. A three electrode set-up was used with the working electrode corresponding to the exposed area defined by the size of the glass microcapillary. Microcapillaries of 100 ± 15 μm diameter were employed. The counter electrode was a platinum wire while an Ag/AgCl, KCl sat. electrode was used as reference. All electrodes were connected to a potentiostat/galvanostat able to measure currents in the range of fA. Open circuit potential measurements were carried out for 5 min. Potentiodynamic anodic polarization curves were then acquired. A scan rate of 1 mV s^{-1} was used. All micro-electrochemical measurements were performed in a 0.01 M NaCl solution. In order to obtain reliable results, for each condition, at least ten measurements were carried out. The solution in the capillary was refreshed before each measurement.

In this work, the total area of scratched samples was firstly immersed in 0.01 M NaCl solution in order to induce the release of the corrosion inhibitor. The sample was rinsed and the micro-cell was then positioned inside the scratch on the bare metal to highlight the presence of an inhibitive layer. A normalized tool (Elcometer 1538 DIN) with a 0.5 mm cutter was used to scratch samples for this technique in order to obtain a perfectly flat surface and a sufficient width to position the glass micro-cell.

3. Results and discussion

3.1. EIS: evolution of barrier and anticorrosion properties

EIS was used to estimate barrier and anticorrosion properties of unscratched coating systems (with and without benzotriazole). Figs. 1 and 2 show the electrochemical response in the form of Bode plots for different immersion times for undoped and doped samples,

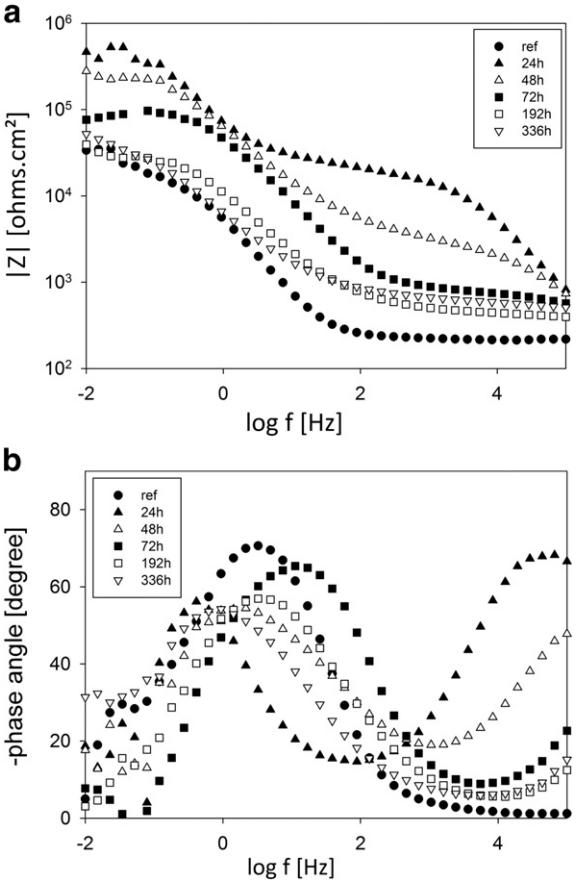

Fig. 1. Bode plots in modulus (a) and in phase (b) for bare AA2024 after 1 h of immersion (ref) and the undoped coating system after different immersion times in 0.05 M NaCl solution.

respectively. The electrochemical response corresponding to the bare AA2024 after 1 h of immersion is added as a reference (ref).

After 24 h of immersion, the coating system doped with benzotriazole shows the highest corrosion protection with an impedance modulus value around 2×10^7 Ω·cm^2 at 0.01 Hz. The low frequency impedance modulus in the case of the undoped coating system is about two orders of magnitude lower in comparison with the benzotriazole doped sample. The anticorrosion protection is considerably improved when benzotriazole molecules are hosted in the mesoporous film. For both systems, the low-frequency modulus decreases with immersion time but more slowly for the doped sample, demonstrating the positive effect due to the presence of the inhibitor. For the undoped sample, the protection brought by the coating is no more visible after 192 h of immersion. By contrast, the corrosion protection is maintained until 768 h of immersion for the doped mesoporous film and the low-frequency modulus is still one order of magnitude higher than that for bare AA2024 for this immersion time.

From a phase perspective, two main time constants are observed. However the presence of a developing additional time constant at low frequencies cannot be excluded for the undoped coating system for long immersion times. The time constant in the high frequency range (about 10^4 Hz) can be related to the coating while the time constant in the medium frequency range (about 5 Hz) is probably the result of the native oxide layer that might be reinforced by the presence of the mesoporous film [36]. The latter is not represented as a separate time constant probably due to the low resistance of the layer induced by its low thickness (250 nm) and high porosity (about 40 vol.%). As a consequence, the mesoporous film cannot be distinguished from the top coat or from the natural oxide layer present on the alloy surface. By comparing undoped and doped coating systems, it is noticeable that the

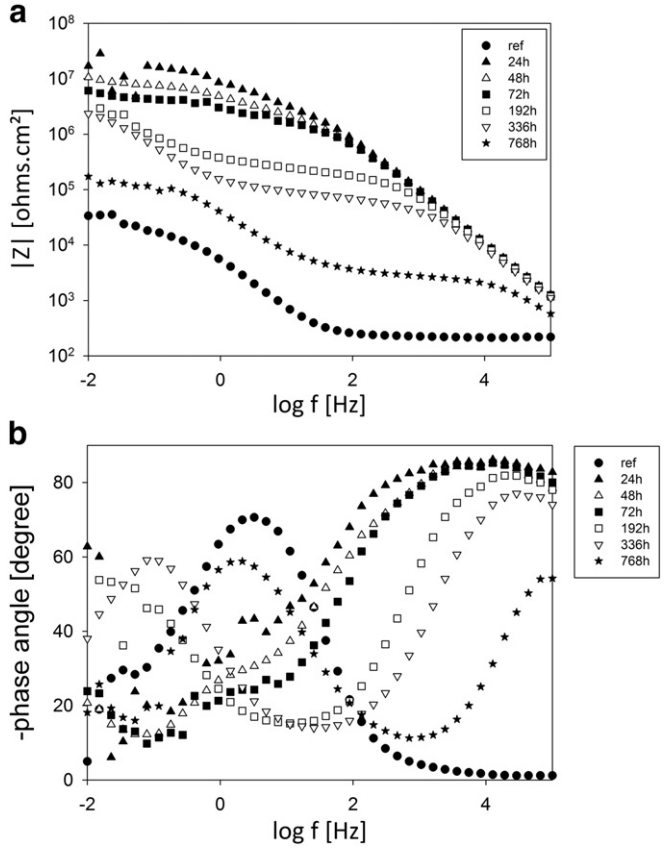

Fig. 2. Bode plots in modulus (a) and in phase (b) for bare AA2024 after 1 h of immersion (ref) and the doped coating system after different immersion times in 0.05 M NaCl solution.

electrochemical response of the coating is different when benzotriazole is incorporated in the mesoporous film. The time constant related to the coating is indeed visible until 768 h of immersion while this one is shifted towards higher frequencies for the undoped sample due to the decrease in the coating resistance for this system. The behaviour in the low frequency range is also different. The time constant related to the oxide layer appears more quickly for the undoped system, demonstrating the weak anticorrosion protection brought to the metal.

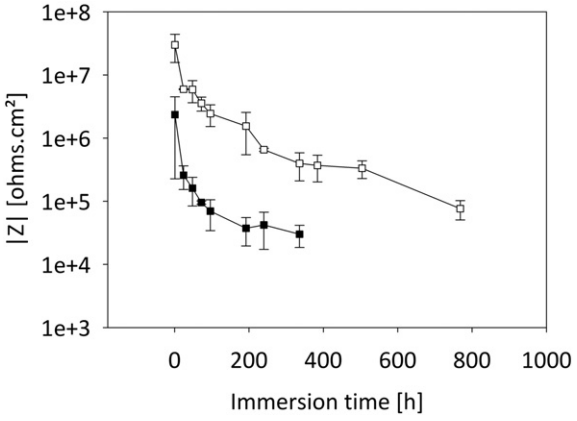

Fig. 3. Evolution of the impedance modulus measured at 0.1 Hz with immersion time in 0.05 M NaCl solution for undoped (■) and doped (□) coating systems. Standard deviations are calculated on the basis of three different samples.

The evolution of the low frequency (10^{-1} Hz) impedance modulus with immersion time is also reported in Fig. 3 for both types of samples to compare their corrosion protection performance and especially to show the good reproducibility of measurements.

The higher corrosion protection observed for the doped sample could be explained either by a better adhesion and compatibility of the top coat on the mesoporous film when benzotriazole molecules are incorporated in mesopores. Another hypothesis would be that the corrosion inhibitor seals the porosity of the mesoporous film after impregnation, increasing its resistance and so the global coating resistance.

Only based on EIS measurements, it is not possible to relate the improvement of the corrosion protection to a self-healing effect due to benzotriazole. In order to ascertain the ability of the system to provide an active protection to the metal, scratched samples were also studied with different local electrochemical techniques.

3.2. Local electrochemical evaluation of self-healing ability

3.2.1. SECM results

In order to highlight the role of benzotriazole in the enhancement of the corrosion protection observed for the doped samples with EIS, SECM measurements were performed on scratched samples in 0.01 M NaCl. The redox competition mode described in [4,40,58] was used to localize corrosion processes. In this mode, the electrochemically active species (namely the dissolved oxygen in the solution) followed at the tip are also involved in the corrosion reactions. During the corrosion process of AA2024 in neutral environment, the dissolution of aluminium is indeed associated with the reduction of the dissolved oxygen in solution (Eq. (1)).

$$O_2 + 2H_2O + 4e^- \rightarrow 4OH^- \quad (1)$$

A competition for the same redox species in the solution between the tip and the sample is thus established. The more oxygen is involved in corrosion reactions, the less oxygen is reduced at the tip, leading to lower currents at the tip.

SECM images of scratched undoped and doped coating systems after 20 h of immersion in 0.01 M NaCl are shown in Fig. 4(a) and (b) respectively. Maps are represented in the form of the normalized current corresponding to the ratio of the tip current to the limiting current. This normalization is mandatory to avoid the influence of the initial concentration in dissolved oxygen present in the aggressive solution. This quantity is dependent upon the solution temperature, aeration etc. and influences the current measured at the tip independently of corrosion processes.

Corrosion activity is detected for the undoped sample. The tip current is lower along the scratch compared to the coating, which indicates a decrease in the concentration of oxygen in this area as a consequence of cathodic processes in the coating defect. The current at the SECM tip measured above the coating is about 60% of the limiting current, suggesting that the protective function of the coating is not ensured anymore after 20 h of immersion in the aggressive solution. This observation is in good agreement with EIS results previously discussed. Corrosion processes are even more marked inside the scratch with a normalized tip current in the order of 30%.

Very interestingly for the doped coating system a very dissimilar SECM map is obtained. After 20 h of immersion in NaCl solution the scratched area is no longer visible and the current decreases progressively with the scan from 80% of the limiting current till 50%. Cyclic voltammograms were recorded far from the sample surface for different immersion times to understand this behaviour. Results are reported in Fig. 5(a) and (b) for undoped and doped samples respectively.

Voltammograms recorded just after the beginning of immersion (0 min) depict a single voltammetric wave which corresponds to

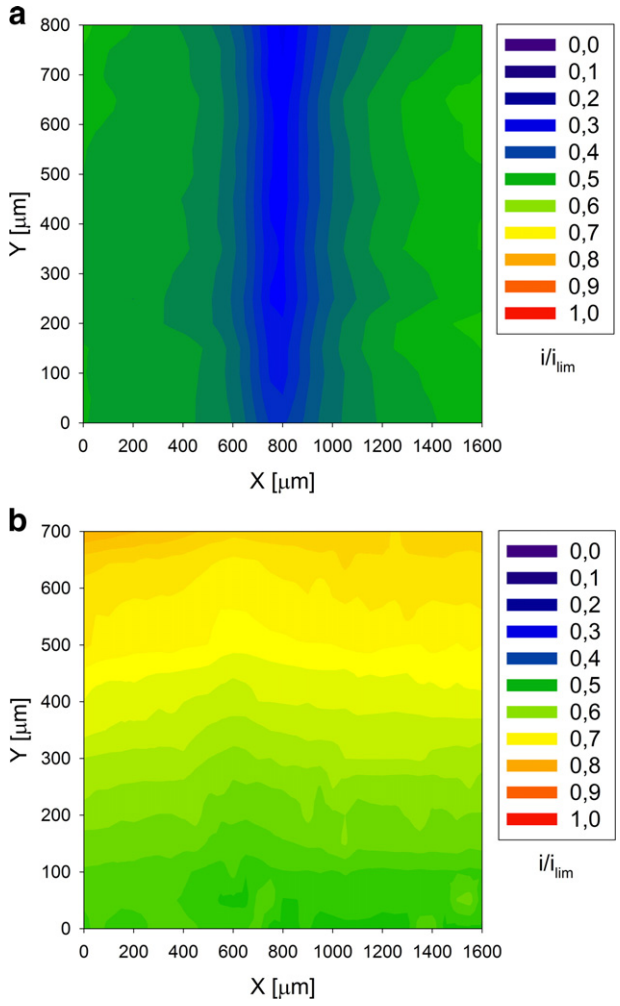

Fig. 4. SECM images of undoped (a) and doped (b) coating systems after 20 h of immersion in 0.01 M NaCl solution containing 5 mM ferrocenemethanol. The scale is expressed in normalized current measured at the tip. The coating defect is located at x = 800 µm for the undoped coating system and at x = 500 µm for the doped coating system.

ferrocenemethanol oxidation. A limiting current is observed for potential values higher than 0.25 V/Ag/AgCl due to a diffusion-limited reaction at the ultramicroelectrode (Eq. (2)).

$$i_{lim} = 4nFCDr \quad (2)$$

In this equation, n is the number of electrons transferred during the oxidation reaction of ferrocenemethanol, F the Faraday constant, C the concentration in ferrocenemethanol, D the diffusion coefficient of ferrocenemethanol in water (1.2×10^{-9} m^2 s^{-1}) and r the tip radius.

For the undoped coating system, cyclic voltammograms are not affected by the immersion time. On the other hand, when the corrosion inhibitor is incorporated in the coating system, a progressive decrease in the limiting current is observed with the elapsed time. This suggests a contamination effect and can be explained by the interaction of benzotriazole molecules with the platinum surface of the tip [59]. Inhibitive species released from the coating system are able to adsorb on platinum resulting in the partial blockage of the sensing tip and thus in a decrease in the active area of the microelectrode. As a consequence, the current measured at the Pt tip is not exclusively related to corrosion processes occurring at the metal surface and precautions have to be taken during SECM measurements. However, although the SECM map is unreliable for the doped sample in terms of relative oxygen concentration determination, the decrease in the tip current observed can still be

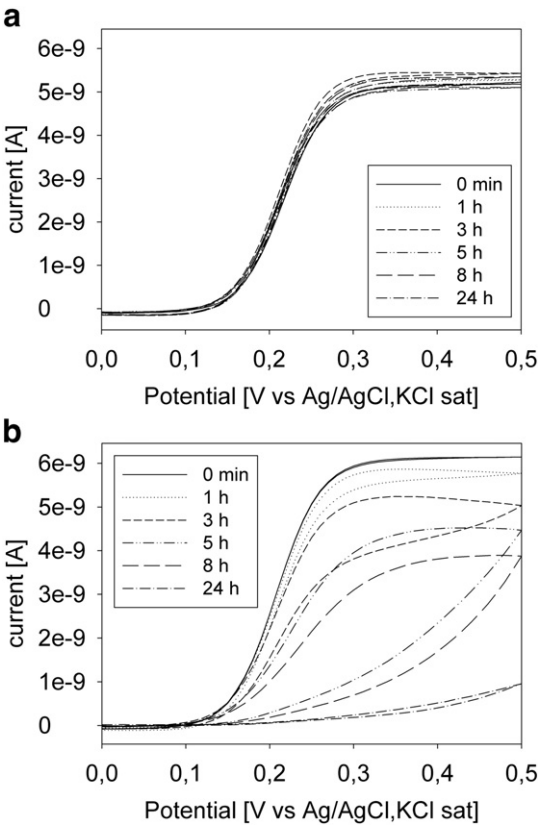

Fig. 5. Cyclic voltammograms measured at the SECM tip in 0.01 M NaCl solution containing 5 mM ferrocenemethanol for different immersion times for the undoped (a) and doped (b) coating systems.

considered as an indication of the release of inhibitive species from the mesoporous pre-treatment.

In order to overcome problems of tip contamination, the way of performing SECM measurements was modified. Line scans were recorded instead of map scans to minimize the scan time. The tip was also stored outside the solution between each line scan to limit the contact time with benzotriazole. Fig. 6 shows line scans corresponding to undoped and doped samples after 30 min of immersion in 0.01 M NaCl.

The current at the SECM tip decreases above the coating defect for both samples, demonstrating that the oxygen is consumed by corrosion processes in this zone. However, the normalized current is lower in the

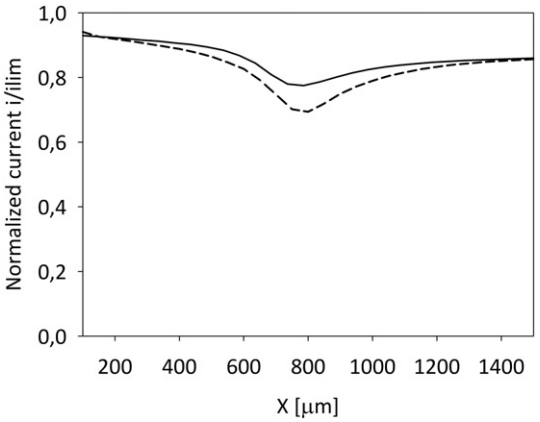

Fig. 6. SECM line scans across the defect after 30 min of immersion in 0.01 M NaCl using dissolved oxygen as electroactive species at the tip ($E_{tip} = -0.77$ V vs Ag/AgCl,KCl sat) for the undoped (dash) and doped (line) coatings.

absence of the corrosion inhibitor which is an indication of faster corrosion reactions.

It is worth mentioning that measurements were performed at three different places along the defect to take into account the homogeneity of phenomena happening inside the scratch. The average value of the normalized current recorded above the defect as well as the standard deviation calculated on the basis of three different samples for each condition are reported according to the immersion time in the aggressive solution in Fig. 7.

At the early stages of immersion, the normalized tip current measured above the coating defect decreases with immersion time for both samples, revealing that corrosion processes in the scratch are not completely inhibited by the presence of benzotriazole. Nevertheless, in the case of the doped coating system, the current drops at a lower rate and tends to stabilize for longer immersion times. This suggests that dissolved oxygen is less consumed by corrosion reactions when inhibitive species are incorporated in the protective coating and that corrosion processes are slower in the defect in that case. By contrast, for the undoped coating system, the progressive decrease in tip current points out that exposure to sodium chloride solution accelerates the corrosion occurring in the defect.

SECM scan lines clearly demonstrate the inhibitive action of benzotriazole molecules released from mesopores in the scratch and the positive effect of the compound on anticorrosion properties of the system. It is also worth noting that the contamination of the tip is no longer observed by performing line scans. As a proof of this fact, Fig. 8 depicts cyclic voltammograms recorded far from the sample surface for different immersion times.

The limiting current is relatively constant along the immersion, suggesting that precautions taken during measurements (line scan and storage of the tip out of the solution between measurements) are sufficient to limit the adsorption of benzotriazole molecules on the SECM tip.

3.2.2. SVET results

The slowdown of corrosion processes inside the scratch for the doped coating system was revealed by SECM measurements. However, as explained previously, interactions observed between benzotriazole and Pt-microelectrode make the scanning of the whole defect unreliable. As a consequence, SVET was used as a second technique to confirm results observed with SECM.

2D current density maps measured after different immersion times and corresponding optical images are presented for the undoped coating system in Fig. 9. Positive values of current density correspond to the anodic activity and negative values to the cathodic activity.

Anodic and cathodic activities are observed above the scratch after immersion of the sample in the aggressive solution. The anodic activity is assigned to the dissolution of the metal while the cathodic activity is related to the reduction reaction of dissolved oxygen. A pitting corrosion site is directly detected after immersion. The current density increases until 4 h of immersion due to corrosion processes and then decreases for longer immersion times. This drop can be associated to the appearance of corrosion products inside the scratch as observed on optical images corresponding to the SVET maps.

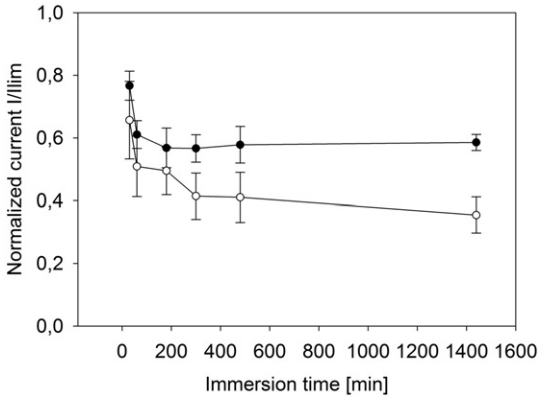

Fig. 7. Evolution with immersion time of the normalized tip current above the scratch for the undoped (○) and the doped (●) coating systems. The tip was stored outside the aggressive solution between consecutive experiments.

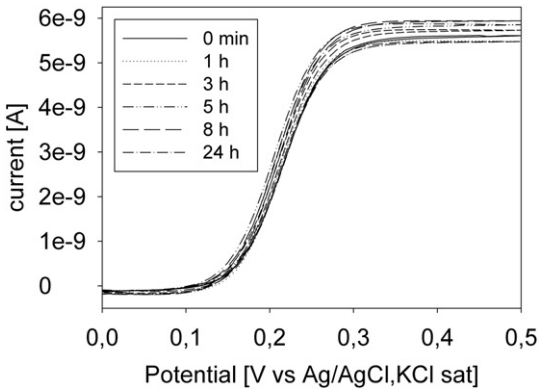

Fig. 8. Cyclic voltammograms measured at the SECM tip in 0.01 M NaCl solution doped with 5 mM ferrocenemethanol for different immersion times for the doped coating system. The tip was stored outside the aggressive solution between consecutive experiments.

The same experiment was carried out for the doped coating system. 2D current density maps measured after different immersion times and corresponding optical images are presented for the doped coating system in Fig. 10.

An obvious slowdown of the activity and as a consequence of the corrosion processes is noticed for samples doped with benzotriazole molecules.

The anodic activity is weaker compared to the undoped sample and the decrease observed after 4 h of immersion is not due, contrarily to the undoped coating, to the appearance of corrosion products. The surface of the metal within the scratch does not show significant corrosion attack during the whole test duration (Fig. 10(e)). This improvement in anticorrosion properties can be related to the corrosion inhibitor incorporated in the coating. It was shown in [39] that the mesoporous film presents an important open pore volume (40% in volume) leading to a high loading content in benzotriazole (8×10^{-7} mol·cm^{-2} of film) and that the corrosion inhibitor is directly leached out in presence of an aqueous environment. When the top coat is not damaged, its presence prevents an undesired leakage of benzotriazole in the electrolyte. In contrast, as soon as the top coat is scratched, mesopores are exposed to the saline solution and benzotriazole is released from the mesoporous silica film in a sufficient amount to partially inhibit corrosion processes occurring on the bare metal.

The trend is similar to the one observed with SECM measurements. However, it is interesting to mention that optically, samples always appear to be more corroded during SECM measurements compared to SVET measurements despite the same aggressive solution (0.01 M NaCl). This is probably due to the undesired influence of the SECM probe measurement on the processes occurring. The reduction of dissolved oxygen is forced at the tip, producing hydroxyl ions and locally modifying the pH of the aggressive solution. These changes can induce a modification in corrosion and protection mechanisms [57,60].

3.3. Electrochemical micro-cell measurements: highlighting the formation of an inhibitive layer inside the scratch

In order to have better insights on the phenomena involved at the substrate surface exposed in the scratched area of the doped coating system, anodic polarization curves were performed at different places inside the defect (Fig. 11). The scratch was made with a 0.5 mm normalized cutter and the diameter of the glass micro-cell surrounded by the

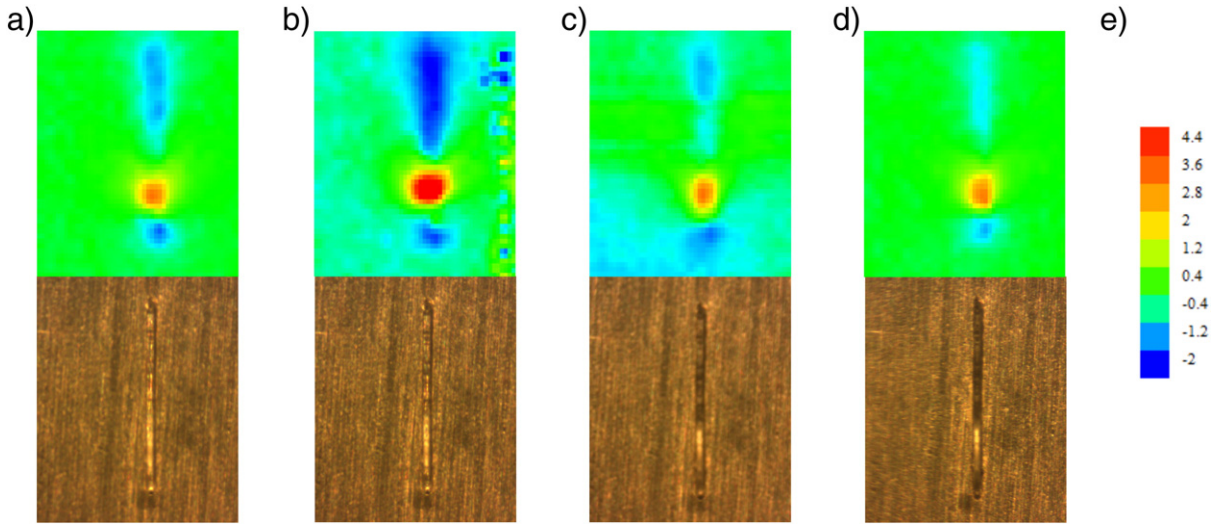

Fig. 9. 2D maps of ionic currents above the defect of the undoped coating system and the corresponding optical images after different immersion times in 0.01 M NaCl: 2 h (a), 4 h (b), 14 h (c) and 24 h (d). The current density scale (e) is expressed in μA/cm^2. The scan size is 2500 μm × 2080 μm and the defect size is 1.9 mm × 75 μm.

silicon gasket was 100 ± 15 μm. Before performing the electrochemical test, the whole area of the sample (coating + defect) was immersed in 0.01 M NaCl in order to induce the release of benzotriazole and the formation of an inhibitive layer. The objective of the polarization curve is to highlight the presence of a protective film inside the defect. Unlike usual microcell measurements [53,54], the set-up used in the present work is not designed to select a specific region on AA2024. Measurements were performed on the bare metal inside the scratch regardless of the underlying microstructure.

Fig. 12 shows anodic potentiodynamic polarization curves in 0.01 M NaCl carried out on distinct regions on the bare metal inside the scratch of the doped coating system before the immersion step (i.e. benzotriazole molecules are still hosted inside mesopores). As explained in Section 2.2, a large number of polarization curves were acquired. The curves displayed in Fig. 12 were selected in order to be representative of all measurements carried out.

The application of a potential more positive than the open circuit potential (OCP) forces the dissolution reaction of aluminium and leads to local damages in the passive oxide film, naturally present on AA2024. A rapid breakdown of the passive layer is observed as a consequence of the pitting phenomenon. Corrosion potentials E_{corr} as well as breakdown potentials E_b are highly scattered probably due to the non-selection of a specific region on AA2024 and due to the small analysed surface areas (7.85×10^{-5} cm^2). Corrosion potentials range from −0.65 V to −0.45 V vs Ag/AgCl, KCl sat. in good agreement with those reported by Paussa et al. [61]. In that work, authors performed electrochemical micro-cell measurements specifically on three different regions of AA2024 and measured the following open circuit potentials: regions rich in Al–Cu–Mg intermetallic particles (−0.75 V vs Ag/AgCl, KCl sat.), regions rich in Al–Cu–Fe–Mn intermetallic particles (−0.32 V vs Ag/AgCl, KCl sat.) and regions with a very small amount of intermetallic particles (−0.44 V vs Ag/AgCl, KCl sat.). In the present

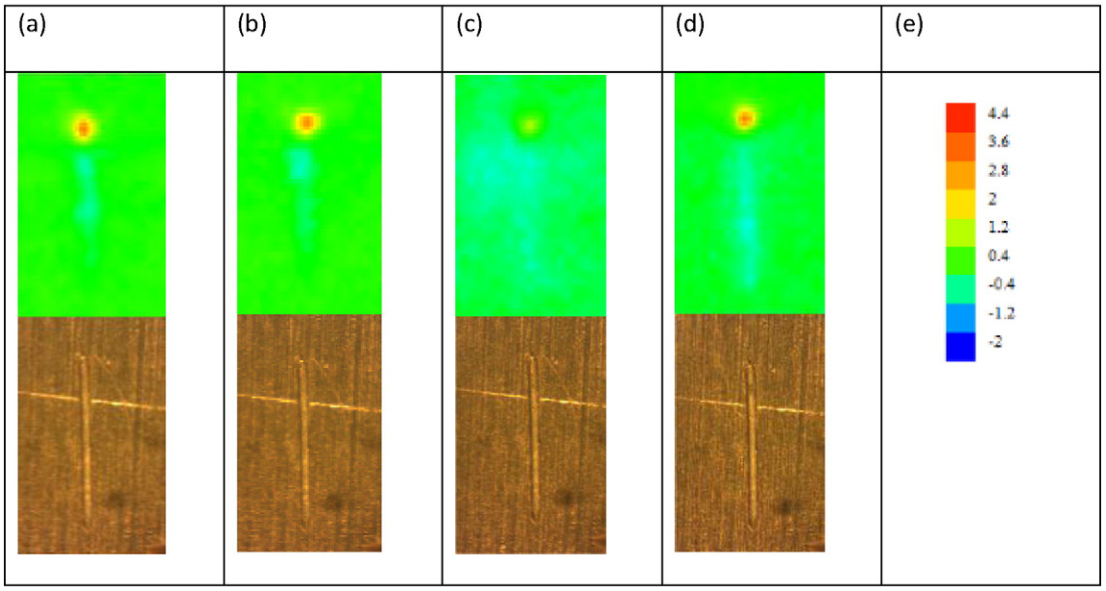

Fig. 10. 2D maps of ionic currents above the defect of the doped coating system and the corresponding optical images after different immersion times in 0.01 M NaCl: 2 h (a), 4 h (b), 14 h (c) and 24 h (d). The current density scale (e) is expressed in μA/cm^2. The scan size is 2160 μm × 1350 μm and the defect size is 1.6 mm × 70 μm.

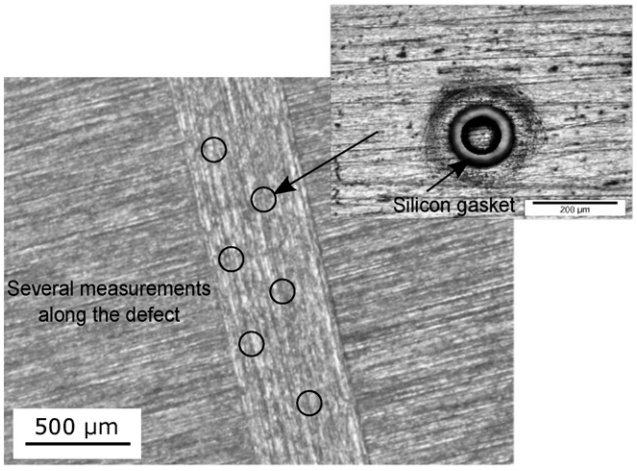

Fig. 11. Optical images of the normalized scratch made on coating and of the silicon gasket surrounding the glass micro-cell.

study, the analysed surface is the combination of all these elements giving accordingly intermediate values of OCP. The difference between corrosion and breakdown potentials is rather low for all curves and the pitting phenomenon happens relatively quickly with the anodic polarization. Corrosion current densities are around 1 $\mu A \cdot cm^{-2}$.

Fig. 13 displays anodic potentiodynamic polarization curves in 0.01 M NaCl solution carried out on distinct regions on the bare metal inside the scratch of the doped coating system after an immersion of 1 h in 0.01 M NaCl solution in order to release benzotriazole molecules from the film. Again, the curves displayed in Fig. 13 were selected to be representative of all measurements carried out. After 1 h of immersion in the aggressive solution, values of corrosion potentials are again too dispersed to determine a clear-cut influence of the corrosion inhibitor on the open circuit potential. However, corrosion current densities are about one order of magnitude lower than those before immersion and a large passive region is observed. The anodic behaviour inside the scratch is therefore considerably improved by the immersion step in the aggressive solution, highlighting the formation of a passive film due to the presence of benzotriazole.

Fig. 14 reports the average value and the standard deviation of corrosion and breakdown potentials based on all measurements for different immersion times in 0.01 M NaCl solution.

Before immersion in the 0.01 M NaCl solution (0 min), the pitting phenomenon on the bare metal inside the scratch occurs directly when the anodic polarization is applied. It is the reason why corrosion and breakdown potentials are almost overlapped taking into account

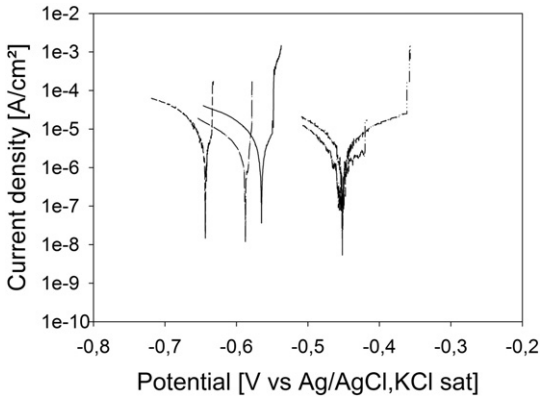

Fig. 12. Local anodic polarization curves acquired using a glass micro-cell of 100 µm in the scratch of the doped coating system before immersion in 0.01 M NaCl solution.

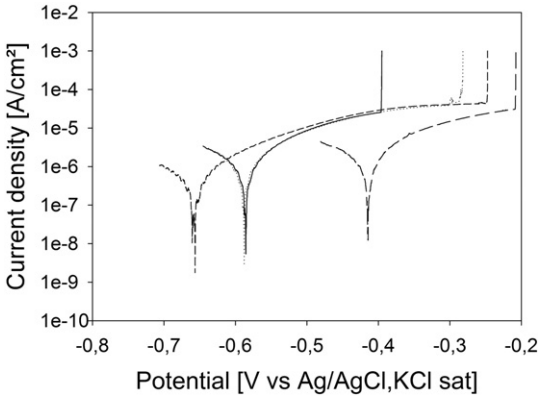

Fig. 13. Local anodic polarization curves in 0.01 M NaCl acquired using a glass micro-cell of 100 µm in the scratch of the doped coating system after 1 h immersion in 0.01 M NaCl solution.

standard deviations. As discussed above, samples immersed in the aggressive solution before electrochemical micro-cell measurements exhibit a more marked difference between both these potentials whatever for 30 min or 1 h of immersion. Thus, the release of benzotriazole from the mesoporous film to the scratched zone seems to decrease the sensitivity to pitting of the bare metal due to a rather fast inhibitive action. This observation is in good agreement with SECM and SVET results and with the well-known ability of benzotriazole to adsorb on the metal surface, reinforcing its natural passive oxide layer [36]. For immersion times longer than 1 h in 0.01 M NaCl solution, local anodic polarization curves are no longer measurable. Indeed, as shown in Fig. 15, several pits are visible inside the defect making the area heterogeneous and the OCP not sufficiently stable to determine a reliable polarization curve. This result underlines the time limited effect of benzotriazole for the active protection of the substrate.

These performance limits have already been detected by SECM and SVET results but are more marked for micro-cell measurements probably due to the size of the defect. For the latter technique, the width of the scratch is adapted to the micro-cell diameter and is about ten times larger than for SECM or SVET measurements. The quantity of benzotriazole released from mesopores is therefore more critical to obtain a homogeneous and stable inhibitive layer on the total surface area exposed in the defect.

The positive effect brought by benzotriazole can also be highlighted on the basis of optical pictures taken after 30 min of immersion in 0.01 M NaCl for undoped and doped coating systems (Fig. 16).

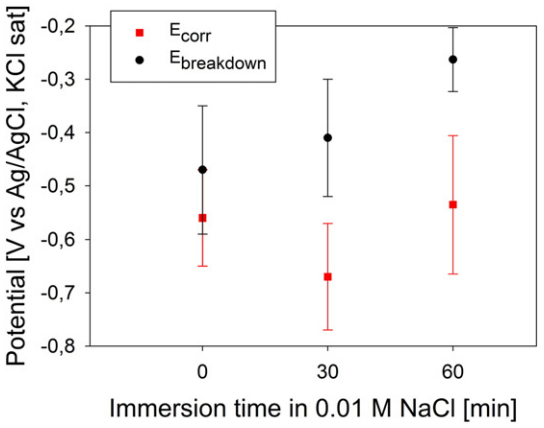

Fig. 14. Corrosion (■) and breakdown (●) potentials measured by means of the electrochemical micro-cell inside the scratch of the doped coating system for different immersion times in 0.01 M NaCl solution.

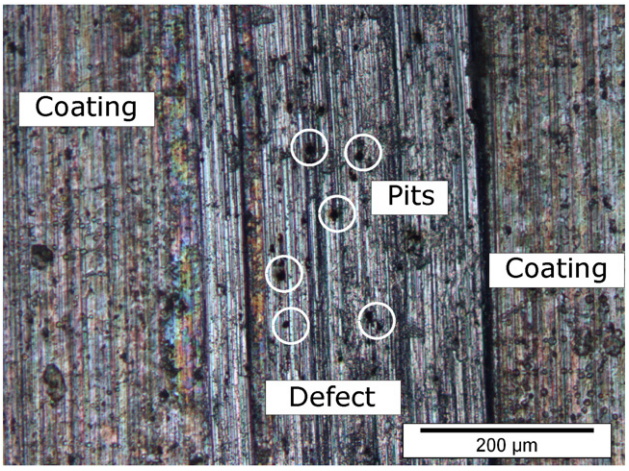

Fig. 15. Optical photo of the scratched doped coating system after 2 h of immersion in 0.01 M NaCl solution.

In the absence of the corrosion inhibitor, the pitting phenomenon is observed on the sample surface while the metal exposed in the scratch for the doped coating system is not damaged. The fast appearance of pits inside the scratch also explains why micro-cell measurements were not possible for the undoped coating system even after relatively short immersion times.

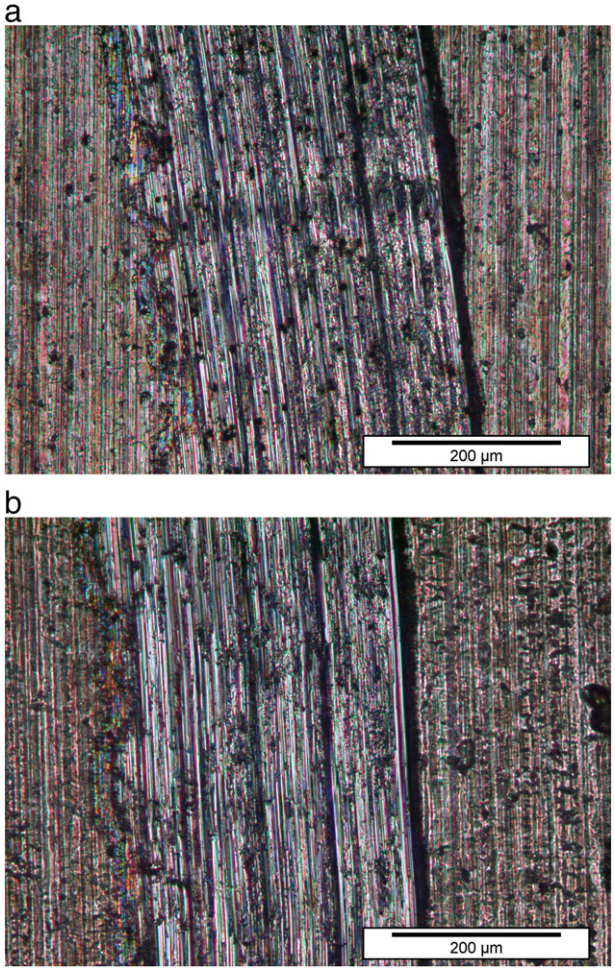

Fig. 16. Optical photos of the scratched undoped (a) and doped (b) coating systems after 30 min of immersion in 0.01 M NaCl solution.

4. Conclusions

Results presented in the present paper clearly confirm the formation of an inhibitive film leading to slower corrosion processes in a coating defect in case a benzotriazole doped mesoporous silica pretreatment is applied. Benzotriazole molecules are directly released from the mesoporous silica pretreatment once the top coat is damaged and act rapidly to protect the bare metal and to delay the initial stages of corrosion. The potential of these two-layer coating systems to offer an active protection to AA2024 aluminium alloys is confirmed by complementary macro- and microscopic electrochemical techniques.

The use of an electrochemical micro-cell was demonstrated to be a useful technique to evaluate a self-healing action of a coating in an artificial defect. The formation of a protective film on the bare metal was proved by the appearance of a passive region in anodic polarization curves.

Although the positive effect of the corrosion inhibitor has been revealed, the corrosion protection was not ensured for long immersion times when the coating system is scratched. The limited quantity of corrosion inhibitor released from the mesoporosity and its lower inhibitive action when the compound is not present in excess in the aggressive solution might explain the time-limited efficiency of the system. In order to enhance the long-term corrosion protection, the mesoporous silica pretreatment doped with benzotriazole could be combined with a more advanced top coat system, such as a self-healing polymer coating. The action of the corrosion inhibitor could delay corrosion processes occurring inside the defect during the period required by the polymer to recover its initial barrier properties.

Acknowledgements

Isaline Recloux wishes to thank the FRIA (Fonds pour la Formation à la Recherche dans l'Industrie et l'Agriculture) for funding. This study was also done in the framework of the Opti^{2}mat and Flycoat "Programmes d'Excellence" financed by the Walloon Region (Belgium).

References

[1] E. Eichinger, J. Osborne, T. Van Cleave, Hexavalent chromium elimination: an aerospace industry progress report, Met. Finish. 95 (1997) 36–41.
[2] Regulation (EC) No 1907/2006, Official Journal of the European Union L 396 of 30 December 2006(DOI) 2006.
[3] M.L. Zheludkevich, S.K. Poznyak, L.M. Rodrigues, D. Raps, T. Hack, L.F. Dick, T. Nunes, M.G.S. Ferreira, Active protection coatings with layered double hydroxide nanocontainers of corrosion inhibitor, Corros. Sci. 52 (2010) 602–611.
[4] Y. González-García, J.M.C. Mol, T. Muselle, I. De Graeve, G. Van Assche, G. Scheltjens, B. Van Mele, H. Terryn, SECM study of defect repair in self-healing polymer coatings on metals, Electrochem. Commun. 13 (2011) 169–173.
[5] R. Naderi, M. Fedel, F. Deflorian, M. Poelman, M. Olivier, Synergistic effect of clay nanoparticles and cerium component on the corrosion behavior of eco-friendly silane sol–gel layer applied on pure aluminum, Surf. Coat. Technol. 224 (2013) 93–100.
[6] T.G. Harvey, S.G. Hardin, A.E. Hughes, T.H. Muster, P.A. White, T.A. Markley, P.A. Corrigan, J. Mardel, S.J. Garcia, J.M.C. Mol, A.M. Glenn, The effect of inhibitor structure on the corrosion of AA2024 and AA7075, Corros. Sci. 53 (2011) 2184–2190.
[7] N. Birbilis, R.G. Buchheit, Inhibition of AA2024-T3 on a phase-by-phase basis using an environmentally benign inhibitor, cerium dibutyl phosphate, Electrochem. Solid-State Lett. 8 (2005) C180–C183.
[8] P.A. White, A.E. Hughes, S.A. Furman, High-throughput channel arrays for inhibitor testing: proof of concept for AA2024-T3, Corros. Sci. 51 (2009) 2279–2290.
[9] T.H. Muster, A.E. Hughes, S.A. Furman, A rapid screening multi-electrode method for the evaluation of corrosion inhibitors, Electrochim. Acta 54 (2009) 3402–3411.
[10] T.A. Markley, M. Forsyth, A.E. Hughes, Corrosion protection of AA2024-T3 using rare earth diphenyl phosphates, Electrochim. Acta 52 (2007) 4024–4031.
[11] M. Garcia-Heras, A. Jimenez-Morales, B. Casal, J.C. Galvan, S. Radzki, M.A. Villegas, Preparation and electrochemical study of cerium–silica sol–gel thin films, J. Alloys Compd. 380 (2004) 219–224.
[12] W. Trabelsi, E. Triki, L. Dhouibi, M.G.S. Ferreira, M.L. Zheludkevich, M.F. Montemor, The use of pre-treatments based on doped silane solutions for improved corrosion resistance of galvanised steel substrates, Surf. Coat. Technol. 200 (2006) 4240–4250.
[13] A.F. Galio, S.V. Lamaka, M.L. Zheludkevich, L.F.P. Dick, I.L. Müller, M.G.S. Ferreira, Inhibitor-doped sol–gel coatings for corrosion protection of magnesium alloy AZ31, Surf. Coat. Technol. 204 (2010) 1479–1486.

[14] D. Raps, T. Hack, J. Wehr, M.L. Zheludkevich, A.C. Bastos, M.G.S. Ferreira, O. Nuyken, Electrochemical study of inhibitor-containing organic–inorganic hybrid coatings on AA2024, Corros. Sci. 51 (2009) 1012–1021.
[15] N.N. Voevodin, N.T. Grebasch, W.S. Soto, F.E. Arnold, M.S. Donley, Potentiodynamic evaluation of sol–gel coatings with inorganic inhibitors, Surf. Coat. Technol. 140 (2001) 24–28.
[16] W. Trabelsi, P. Cecilio, M.G.S. Ferreira, M.F. Montemor, Electrochemical assessment of the self-healing properties of Ce-doped silane solutions for the pre-treatment of galvanised steel substrates, Prog. Org. Coat. 54 (2005) 276–284.
[17] J. Mardel, S.J. Garcia, P.A. Corrigan, The characterisation and performance of Ce (dbp) 3-inhibited epoxy coatings, Prog. Org. Coat. 70 (2011) 91–101.
[18] D. Borisova, H. Möhwald, D.G. Shchukin, Mesoporous silica nanoparticles for active corrosion protection, ACS Nano 5 (2011) 1939–1946.
[19] F. Maia, J. Tedim, A.D. Lisenkov, A.N. Salak, M.L. Zheludkevich, M.G.S. Ferreira, Silica nanocontainers for active corrosion protection, Nanoscale 4 (2012) 1287–1298.
[20] M.L. Zheludkevich, D.G. Shchukin, K.A. Yasakau, H. Möhwald, M.G.S. Ferreira, Anticorrosion coatings with self-healing effect based on nanocontainers impregnated with corrosion inhibitor, Chem. Mater. 19 (2007) 402–411.
[21] E.V. Skorb, D. Fix, D.V. Andreeva, H. Möhwald, D.G. Shchukin, Surface-modified mesoporous SiO_2 containers for corrosion protection, Adv. Funct. Mater. 19 (2009) 2373–2379.
[22] J. Tedim, S.K. Poznyak, A. Kuznetsova, D. Raps, T. Hack, M.L. Zheludkevich, M.G.S. Ferreira, Enhancement of active corrosion protection via combination of inhibitor-loaded nanocontainers, ACS Appl. Mater. Interfaces 2 (2010) 1528–1535.
[23] Y.M. Lvov, D.G. Shchukin, H. Möhwald, R.R. Price, Halloysite clay nanotubes for controlled release of protective agents, ACS Nano 2 (2008) 814–820.
[24] D. Fix, D.V. Andreeva, Y.M. Lvov, D.G. Shchukin, H. Möhwald, Application of inhibitor-loaded halloysite nanotubes in active anti-corrosive coatings, Adv. Funct. Mater. 19 (2009) 1720–1727.
[25] D.G. Shchukin, S.V. Lamaka, K.A. Yasakau, M.L. Zheludkevich, M.G.S. Ferreira, H. Mohwald, Active anticorrosion coatings with halloysite nanocontainers, J. Phys. Chem. C 112 (2008) 958–964.
[26] E. Abdullayev, R. Price, D. Shchukin, Y. Lvov, Halloysite tubes as nanocontainers for anticorrosion coating with benzotriazole, ACS Appl. Mater. Interfaces 1 (2009) 1437–1443.
[27] S.A.S. Dias, S.V. Lamaka, C.A. Nogueira, T.C. Diamantino, M.G.S. Ferreira, Sol–gel coatings modified with zeolite fillers for active corrosion protection of AA2024, Corros. Sci. 62 (2012) 153–162.
[28] C. Motte, M. Poelman, A. Roobroeck, Improvement of corrosion protection offered to galvanized steel by incorporation of lanthanide modified nanoclays in silane layer, Prog. Org. Coat. 74 (2012) 326–333.
[29] M.F. Montemor, D.V. Snihirova, M.G. Taryba, Self-healing ability in protective coatings modified with combinations of layered double hydroxides and cerium molibdate nanocontainers filled with corrosion inhibitors, Electrochim. Acta 60 (2012) 31–40.
[30] J. Tedim, M.L. Zheludkevich, Nanostructured LDH-container layer with active protection functionality, J. Mater. Chem. 21 (2011) 15464–15470.
[31] M.G.S. Ferreira, R.G. Duarte, M.F. Montemor, A.M.P. Simoes, Silanes and rare earth salts as chromate replacers for pre-treatments on galvanised steel, Electrochim. Acta 49 (2004) 2927–2935.
[32] N.C. Rosero-Navarro, L. Paussa, F. Andreatta, Y. Castro, A. Duran, M. Aparicio, L. Fedrizzi, Optimization of hybrid sol–gel coatings by combination of layers with complementary properties for corrosion protection of AA2024, Prog. Org. Coat. 69 (2010) 167–174.
[33] S. Lamaka, M. Zheludkevich, K. Yasakau, R. Serra, S. Poznyak, M. Ferreira, Nanoporous titania interlayer as reservoir of corrosion inhibitors for coatings with self-healing ability, Prog. Org. Coat. 58 (2007) 127–135.
[34] S.V. Lamaka, M.L. Zheludkevich, K.A. Yasakau, M.F. Montemor, P. Cecílio, M.G.S. Ferreira, TiOx self-assembled networks prepared by templating approach as nanostructured reservoirs for self-healing anticorrosion pre-treatments, Electrochem. Commun. 8 (2006) 421–428.
[35] F. Khelifa, M.E. Druart, Y. Habibi, F. Bénard, P. Leclère, M.-G. Olivier, Ph. Dubois, Sol–gel incorporation of silica nanofillers for tuning the anti-corrosion protection of acrylate-based coatings, Prog. Org. Coat. 76 (2013) 900–911.
[36] M.L. Zheludkevich, K.A. Yasakau, S.K. Poznyak, M.G.S. Ferreira, Triazole and thiazole derivatives as corrosion inhibitors for AA2024 aluminium alloy, Corros. Sci. 47 (2005) 3368–3383.
[37] V. Palanivel, Y. Huang, W.J. van Ooij, Effects of addition of corrosion inhibitors to silane films on the performance of AA2024-T3 in a 0.5 M NaCl solution, Prog. Org. Coat. 53 (2005) 153–168.
[38] A.C. Balaskas, M. Curioni, G.E. Thompson, Effectiveness of 2-mercaptobenzothiazole, 8-hydroxyquinoline and benzotriazole as corrosion inhibitors on AA 2024-T3 assessed by electrochemical methods, Surf. Interface Anal. (2015) (DOI).
[39] I. Recloux, M. Mouanga, M.-E. Druart, Y. Paint, M.-G. Olivier, Silica mesoporous thin films as containers for benzotriazole for corrosion protection of 2024 aluminium alloys, Appl. Surf. Sci. 346 (2015) 124–133.
[40] Y. González-García, S.J. García, A combined redox-competition and negative-feedback SECM study of self-healing anticorrosive coatings, Electrochem. Commun. 13 (2011) 1094–1097.
[41] A.C. Bastos, O.V. Karavai, M.L. Zheludkevich, K.A. Yasakau, M.G.S. Ferreira, Localised measurements of pH and dissolved oxygen as complements to SVET in the investigation of corrosion at defects in coated aluminum alloy, Electroanalysis 22 (2010) 2009–2016.
[42] R.M. Souto, L. Fernández-Mérida, S. González, SECM imaging of interfacial processes in defective organic coatings applied on metallic substrates using oxygen as redox mediator, Electroanalysis 21 (2009) 2640–2646.
[43] A.C. Bastos, A.M. Simões, Application of the scanning electrochemical microscope to the examination of organic coatings on metallic substrates, Prog. Org. Coat. 53 (2005) 177–182.
[44] R.M. Souto, Y. González-Garcıa, Damage to paint coatings caused by electrolyte immersion as observed in situ by scanning electrochemical microscopy, Corros. Sci. 46 (2004) 2621–2628.
[45] R.M. Souto, Y. González-Garcıa, S. González, In situ monitoring of electroactive species by using the scanning electrochemical microscope. Application to the investigation of degradation processes at defective, Corros. Sci. 47 (2005) 3312–3323.
[46] M.L. Zheludkevich, K.A. Yasakau, A.C. Bastos, O.V. Karavai, M.G.S. Ferreira, On the application of electrochemical impedance spectroscopy to study the self-healing properties of protective coatings, Electrochem. Commun. 9 (2007) 2622–2628.
[47] D.V. Andreeva, D. Fix, Self-healing anticorrosion coatings based on pH-sensitive polyelectrolyte/inhibitor sandwichlike nanostructures, Adv. Mater. 20 (2008) 2789–2794.
[48] D.G. Shchukin, M. Zheludkevich, Layer-by-layer assembled nanocontainers for self-healing corrosion protection, Adv. Mater. 18 (2006) 1672–1678.
[49] T. Suter, H. Böhni, A new microelectrochemical method to study pit initiation on stainless steels, Electrochim. Acta 42 (1997) 3275–3280.
[50] F. Andreatta, M.M. Lohrengel, H. Terryn, J.H.W.D. Wit, Electrochemical characterisation of aluminium AA7075-T6 and solution heat treated AA7075 using a micro-capillary cell, Electrochim. Acta 48 (2003) 3239–3247.
[51] F. Andreatta, H. Terryn, J.H.W.D. Wit, Corrosion behaviour of different tempers of AA7075 aluminium alloy, Electrochim. Acta 49 (2004) 2851–2862.
[52] N. Birbilis, R.G. Buchheit, Investigation and discussion of characteristics for intermetallic phases common to aluminum alloys as a function of solution pH, J. Electrochem. Soc. 155 (2008) C117–C126.
[53] L. Paussa, F. Andreatta, D. De Felicis, E. Bemporad, L. Fedrizzi, Investigation of AA2024-T3 surfaces modified by cerium compounds: a localized approach, Corros. Sci. 78 (2014) 215–222.
[54] F. Andreatta, M.E. Druart, A. Lanzutti, M. Lekka, D. Cossement, M.G. Olivier, L. Fedrizzi, Localized corrosion inhibition by cerium species on clad AA2024 aluminium alloy investigated by means of electrochemical micro-cell, Corros. Sci. 65 (2012) 376–386.
[55] K.D. Ralston, T.L. Young, R.G. Buchheit, Electrochemical evaluation of constituent intermetallics in aluminum alloy 2024-T3 exposed to aqueous vanadate inhibitors, J. Electrochem. Soc. 156 (2009) C135–C146.
[56] I. Recloux, M. Debliquy, A. Baroni, Y. Paint, A. Lanzutti, L. Fedrizzi, M.-G. Olivier, Optimization of synthesis parameters of mesoporous silica sol–gel thin films for application on 2024 aluminum alloy substrates, Appl. Surf. Sci. 277 (2013) 201–210.
[57] L.C. Abodi, Y. Gonzalez-Garcia, O. Dolgikh, C. Dan, D. Deconinck, J.M.C. Mol, H. Terryn, J. Deconinck, Simulated and measured response of oxygen SECM-measurements in presence of a corrosion process, Electrochim. Acta 146 (2014) 556–563.
[58] J.J. Santana, J. González-Guzmán, L. Fernández-Mérida, S. González, R.M. Souto, Visualization of local degradation processes in coated metals by means of scanning electrochemical microscopy in the redox competition mode, Electrochim. Acta 55 (2010) 4488–4494.
[59] J. Izquierdo, J.J. Santana, S. González, R.M. Souto, Uses of scanning electrochemical microscopy for the characterization of thin inhibitor films on reactive metals: the protection of copper surfaces by benzotriazole, Electrochim. Acta 55 (2010) 8791–8800.
[60] M.G. Taryba, K.V.d. Bergh, J.D. Strycker, Novel use of a micro-optode in overcoming the negative influence of the amperometric micro-probe on localized corrosion measurements, Corros. Sci. 95 (2015) 36–41.
[61] L. Paussa, F. Andreatta, N.C. Rosero Navarro, A. Durán, L. Fedrizzi, Study of the effect of cerium nitrate on AA2024-T3 by means of electrochemical micro-cell technique, Electrochim. Acta 70 (2012) 25–33.